Electronic structures of air-exposed few-layer black phosphorus by optical spectroscopy

Fanjie Wang, Guowei Zhang, Shenyang Huang, Chaoyu Song, Chong Wang, Qiaoxia Xing, Yuchen Lei, and Hugen Yan[*]

*Department of Physics, State Key Laboratory of Surface Physics and Key Laboratory of Micro and Nano Photonic Structures
(Ministry of Education), Fudan University, Shanghai 200433, China*

The electronic structure of few-layer (FL) black phosphorus (BP) sensitively depends on the sample thickness, strain, and doping. We show that it is also vulnerable to air exposure. The oxidation of BP caused by air exposure gives several optical signatures, including the broadening of resonance peaks and increased Stokes shift between infrared (IR) absorption and photoluminescence (PL) peaks. More importantly, air exposure causes blueshifts of all resonance peaks in IR absorption and PL spectra, with more prominent effects for thinner samples and higher-order subband transitions. Our study alludes to a convenient and exotic way for band-structure engineering of FL-BP through controllable air exposure or defect creation.

I. INTRODUCTION

Black phosphorus (BP) has been demonstrated as a promising candidate for electronic and photonic devices [1–3], benefiting from its unique physical properties such as in-plane anisotropy [4,5], widely tunable direct band gap from the mid-infrared to visible frequency range [6–8], and relatively high carrier mobility [9,10]. Unfortunately, the unpaired electron on the surface makes it reactive to air, causing degradation in samples. Although the mechanism of degradation is still inconclusive, a growing consensus shows photo-oxidation, aided by moisture, is the main cause [11–15]. In particular, ultraviolet photons play a major role [16]. Oxygen breaks the P-P bonds and irreversibly converts BP into P_xO_y compounds. Moisture accelerates the subsequent decomposition of P_xO_y. BP's instability in air hampers the characterization of its intrinsic properties and its device performance. Therefore, it is essential to interrogate the physical consequences of air exposure.

The respective influence of light, oxygen, and humidity on the degradation of few-layer (FL) black phosphorus (BP) has already been addressed in recent studies [17–26]. Corresponding impacts have also been studied by atomic force microscopy (AFM), x-ray photoelectron spectroscopy (XPS), and Raman spectroscopy, showing that many visible bubbles appear on the surface after a certain time of exposure to air, with remarkably reduced intensity ratio of A_g^1/A_g^2 Raman modes [27]. However, AFM can only be used for the surface topography identification, which is not suitable for the early-stage diagnostics. In addition, caution must be taken when characterizing the degradation by Raman spectroscopy. Due to many independent variables such as lattice orientation, thickness, and excitation wavelengths, the Raman response shows complicated behaviors and contradictions still exist [28–31]. Though many efforts have been devoted to exploring

the mechanisms and products of degradation, little is known regarding the band structure of air-exposed BP.

In this paper, we systematically study the degradation-induced changes in the band structure of mechanically exfoliated FL-BP, using infrared (IR) absorption and photoluminescence (PL) spectroscopy, and insights are gained for the degradation process and its consequences. From the measured IR absorption and PL spectra, we can directly trace the evolution of the (optical) band gap and higher-order subband transitions. Interestingly, the degradation induces blueshift of all optical resonances, with shift rates that are subband and layer dependent. Clear signs of blueshift show up within a few minutes of air exposure, underlining the rapidity of degradation and the sensitivity of our characterization technique. Our results are expected to provide a reliable and sensitive determination of the band structure in air-exposed BP and pave the way for quick assessment of device quality by optical means. Meanwhile, our study demonstrates a scheme of band-structure engineering through controllable air exposure.

II. EXPERIMENTAL METHODS

FL-BP samples were mechanically exfoliated on a transparent polydimethylsiloxane (PDMS) substrate in a glove box. The layer (L) number was first estimated by optical contrast and further verified by IR absorption spectroscopy. Samples were protected in an enclosed Linkam chamber (Linksy82) with continuously purged nitrogen during the IR absorption and PL measurements.

As an anisotropic material, BP has two characteristic crystal orientations: armchair (AC) and zigzag (ZZ), as illustrated in Fig. 1(a), corresponding to the strongest and weakest optical response, respectively. The strong polarization- and layer-dependent absorption of BP allows for the fast and accurate determination of crystal orientation and layer number by IR absorption spectroscopy [32,33]. In this work, all of the IR absorption spectra were obtained with incident light polarized along the AC direction. Besides, PL spectroscopy was also used for sample characterization with thickness $\leqslant 3L$.
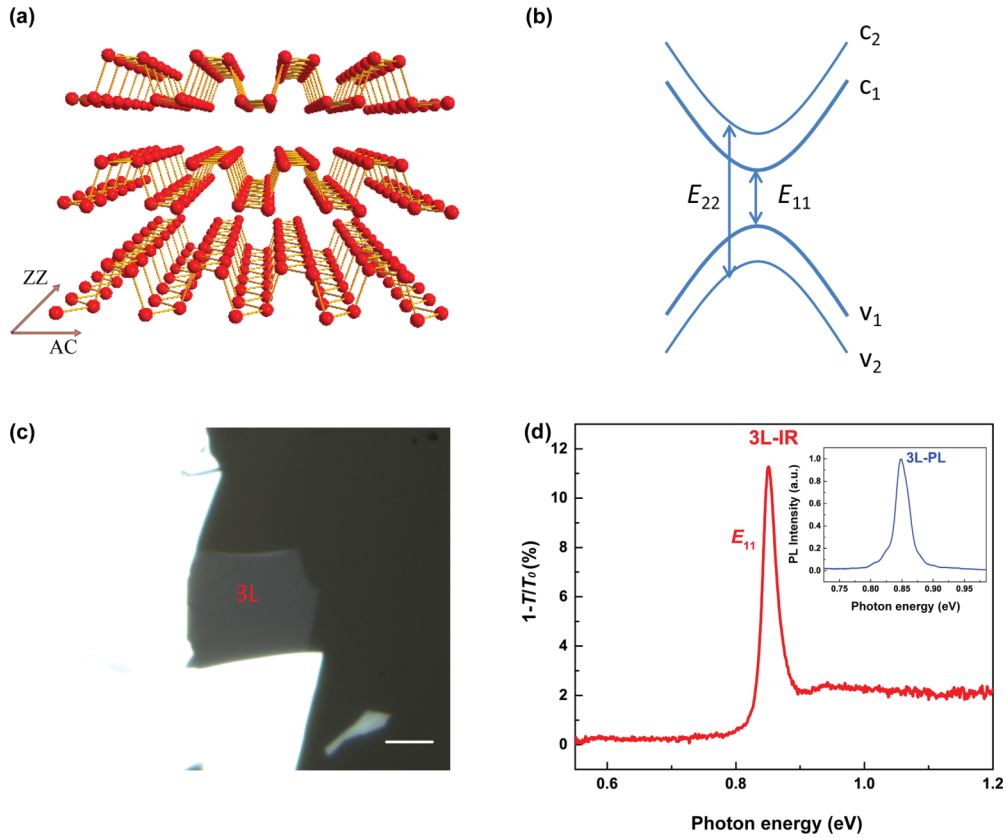
*hgyan@fudan.edu.cn

FIG. 1. Optical characterization of pristine BP samples. (a) Crystal structure of a $3L$ BP. (b) The qualitative energy levels of the $2L$ BP; vertical arrows E_{11} and E_{22} denote transitions $v_1 \rightarrow c_1$ and $v_2 \rightarrow c_2$, respectively. (c) Optical image of a $3L$ BP exfoliated on PDMS. Scale bar: 10 μm. (d) IR absorption spectrum of the $3L$ BP. T_0 and T denote the light transmission of the bare PDMS and the sample on the PDMS, respectively. Inset: PL spectrum of the same $3L$ BP.

All IR absorption spectra of the FL-BP samples were recorded using a Bruker FTIR spectrometer (Vertex 70v) equipped with a Hyperion 2000 microscope. A tungsten halogen lamp was used as the light source to cover the broad spectral range of $3750 - 11\,000$ cm^{-1} (0.36–1.36 eV), in combination with a liquid-nitrogen-cooled MCT detector. The lower-bound cutoff photon energy is restricted by the PDMS substrate. The incident light was focused on BP samples using a 15X IR objective, with the polarization controlled by a broadband ZnSe grid polarizer.

The PL measurements on FL-BP samples were conducted using an Andor AR500i spectrometer equipped with the InGaAs detector, in conjunction with a Nikon microscope and a 50X objective. A 532 nm laser was used for excitation. Samples were kept under the same low laser-excitation power to avoid laser-induced heating and damage during measurements.

III. RESULTS AND DISCUSSIONS

A. Optical characterization of FL-BP

Owing to the layer-layer interactions and quantum confinement in the out-of-plane direction, conduction and valence bands of the N-layer BP split into N 2-dimensional (2D) subbands. As an example, Fig. 1(b) illustrates the simplified band structures of a $2L$ BP, where c_1, c_2 and v_1, v_2 denote the quantized conduction and valence subbands, and the vertical

arrows illustrate the optical transitions between c_1 and v_1, and c_2 and v_2, respectively. Here we define E_{nn} as the nth-order subband transition (transition from v_n to c_n) since interband transitions in symmetric quantum wells with normal light incidence are only allowed for the same subband index n.

Figure 1(d) shows the IR extinction ($1-T/T_0$) spectra of a freshly exfoliated $3L$ BP [the optical image is shown in Fig. 1(c)] on a PDMS substrate, where T_0 and T denote the light transmission through the PDMS without and with BP on it, respectively. Obviously, the IR absorption is dominated by significant exciton effect of the E_{11} transition, as expected in low-dimensional semiconductors, while E_{22} and E_{33} transitions are beyond our measurement range. Moreover, strong PL emission [the inset in Fig. 1(d)] was observed in this sample, with its peak energy (0.85 eV) almost the same as the absorption peak, showing a negligible Stokes shift [see Fig. 4(a)]. This further confirms the high quality of pristine FL-BP samples.

B. Subband- and thickness-dependent blueshift

To characterize the impacts of air exposure on the electronic structure of FL-BP, we monitored the evolution of IR and PL spectra of FL-BP samples in air over time. All samples were deliberately exposed to air for a certain amount of time, and subsequently protected in a chamber by purging nitrogen gas for optical measurements. We checked the effectiveness
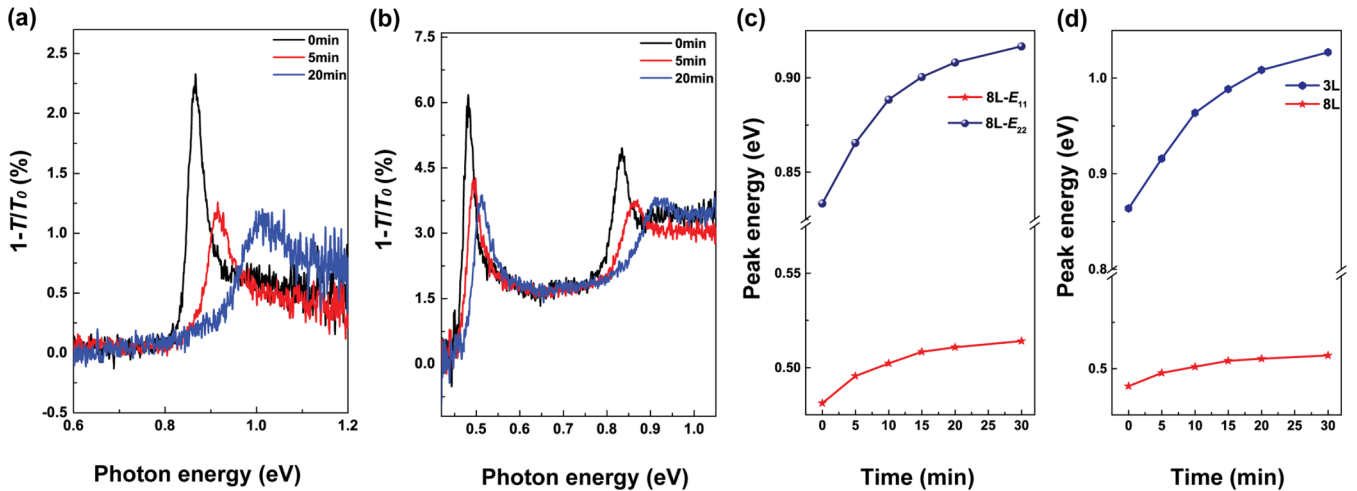
FIG. 2. Subband- and layer-dependent blueshift of (a) $3L$ and (b) $8L$ BP. (c) E_{11} and E_{22} peak energies of the $8L$ sample as a function of exposure time; for the same sample, the E_{22} peak moves faster than E_{11}. (d) E_{11} peak energies of the $3L$ and $8L$ sample extracted from (a) and (b); the $3L$ sample peak moves faster.

of the protection method; the IR absorption spectrum barely changes over time in a nitrogen-gas environment, in striking contrast to air-exposed samples. This confirms the effectiveness of N_2 gas protection and controllable air exposure is feasible. See the Supplemental Material for the efficient nitrogen protection [34].

We first focus on the early stage of the air exposure, in which the BP samples do not visually show any inhomogeneity from a microscope optical image. In the later stage, as discussed in the final part of the paper, the sample thickness will be reduced inhomogeneously. Figures 2(a) and 2(b) show the IR absorption spectra of $3L$ and $8L$ BP in air at different exposure times. Both BP samples were on the same PDMS substrate and the same exposure condition was ensured. For clarity, only three spectra (0, 5, 20 min) are shown here. The IR absorption spectra of fresh BP samples (black curves) exhibit sharp and narrow exciton resonances, associated with optical transitions between quantized valence and conduction subbands. The results indicate that FL-BP samples are very sensitive to air; only a few minutes of exposure cause apparent modification of the sample properties: the remarkable reduced peak height and broadened linewidth [red and blue curves in Figs. 2(a) and 2(b)] are directly attributed to the introduction of defects [35]. More interestingly, the degradation causes apparent blueshift of peaks. Take the $3L$ sample for example, where the resonance peak gradually shifts from 0.87 to 1 eV [Fig. 2(a)]. The scenario reminds us of possible band-structure tuning for FL-BP through defect engineering. The IR spectra are clear indicators of the sample quality. On the contrary, optical microscope images barely show any discernable change at this stage.

Figure 2(c) shows peak energies for E_{11} and E_{22} transitions of the $8L$ BP as a function of exposure time, whose typical spectra are displayed in Fig. 2(b). We can see that E_{22} shifts much faster than E_{11}. Figure 2(d) compares the E_{11} transitions for the $3L$ and $8L$ sample shown in Figs. 2(a) and 2(b), and the $3L$ sample exhibits a more drastic shift. The peak shift can be fairly compared because both $3L$ and $8L$ samples are on the very same substrate and the exposure conditions are always

the same. We performed similar studies for many samples with different thicknesses (see the Supplemental Material for more examples [34]). All measurements show the same qualitative behaviors, i.e., air exposure causes blueshift of all resonance peaks and higher-order subband transitions and thinner samples are more sensitive [36].

The band structure of pristine FL-BP can be approximated as that of an infinite square quantum well. Due to the relatively strong layer-layer interaction, the effective mass of carriers in the perpendicular direction is relatively small. Therefore, the band gap and higher-order optical transitions are sensitive to the sample thickness (quantum well width). By the same token, the band structure will also be sensitive to the modification of quantum well profile induced by the oxidation of the surface layer. During the early stage of the degradation, it is reasonable to assume that only the top layer is partially oxidized and other layers underneath are intact. Therefore, a potential barrier for carriers forms between the top layer and the rest of the sample. The inset in Fig. 3(a) shows the energy diagram of pristine BP and its oxide. Pristine BP acts as a perfect infinite square quantum well. The appearance of oxide modifies the perfect structure and introduces a barrier with height Δ, as shown in Fig. 3(a). This certainly modifies the electronic structure and tunes the optical transitions.

We simulate the blueshift of the optical transitions numerically. We assume the N-1 layers underneath are intact, and only the top layer oxidized homogeneously. The severity of the oxidation is characterized by the barrier height Δ: the larger the barrier, the more severe the oxidation is. We extracted the ground and excited states in this modified quantum well by numerically solving the one-dimensional Schrodinger equation under the effective-mass approximation [4,7] (see the Supplemental Material for details [34]). Figures 3(b) and 3(c) summarize the transition energy versus oxide barrier height, where we assumed the thickness of the oxide layer equals the single-layer BP thickness without loss of generality. As expected, the results are consistent with our experimental findings. First of all, all peaks shift to higher energy since the potential barrier introduced by degradation effectively
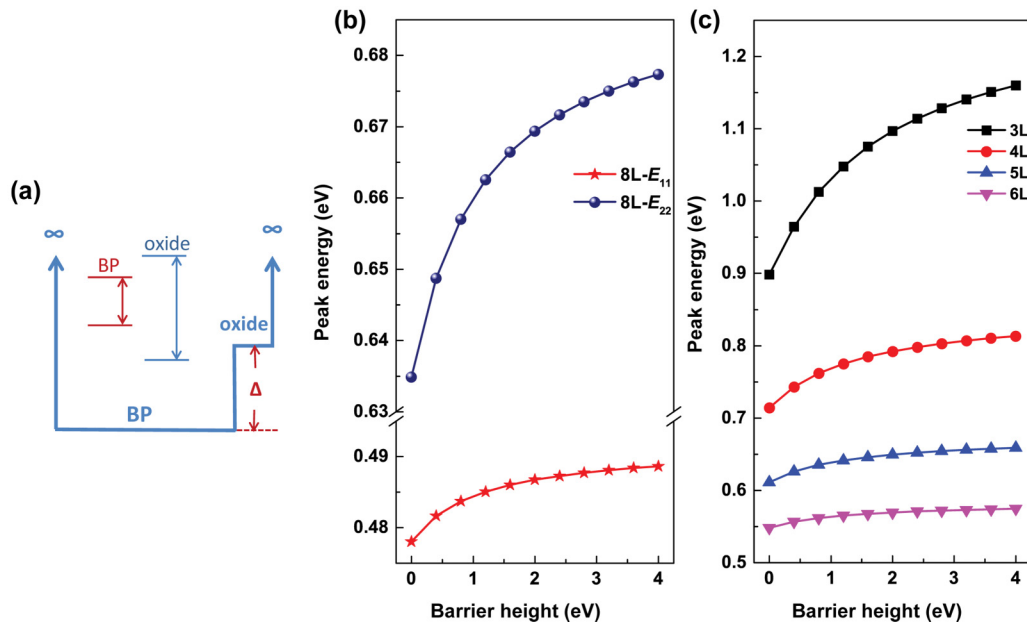
FIG. 3. The mechanism of blueshift. (a) The adjusted quantum well. Inset: The energy diagram of BP and its oxide. Δ denotes the effective barrier height. (b) Calculated E_{11} and E_{22} transition energies of 8L BP as a function of barrier height. (c) Calculated E_{11} peak energies vs the oxide's barrier height for BP with various layer numbers.

enhances the 2D quantum confinement or, equivalently, reduces the effective thickness of the quantum well. Second, the higher-order subband envelope wave function [in the form of sin $(n\pi z/L)$ for a perfect infinite square well, where n is the subband order, L is the sample thickness] has larger amplitude in the vicinity of the degraded surface, and hence the energy eigenvalues of higher-order subbands shift more than that of lower order. This explains the fact that E_{22} shifts faster than E_{11} [Fig. 3(b)] for the same sample. Third, by assuming the same degradation rate of the top layer for different thickness samples, the thinner samples are certainly more sensitive to

degradation and the peaks show higher shift rates than that for thicker samples [Fig. 3(c)]. The simulated results are in very good qualitative agreement with our experimental findings. It should be admitted though, in this model, for simplicity, we assume all few-layer samples have the same degradation rate of the surface layer and this can already explain the faster shift of thinner samples. Of course, this hypothesis deserves caution since theoretical studies have predicted that thinner samples (particularly 1L or 2L) tend to react faster due to a better match between the band gap and oxide energy levels [35,37]. Since the current study does not focus on the thinnest
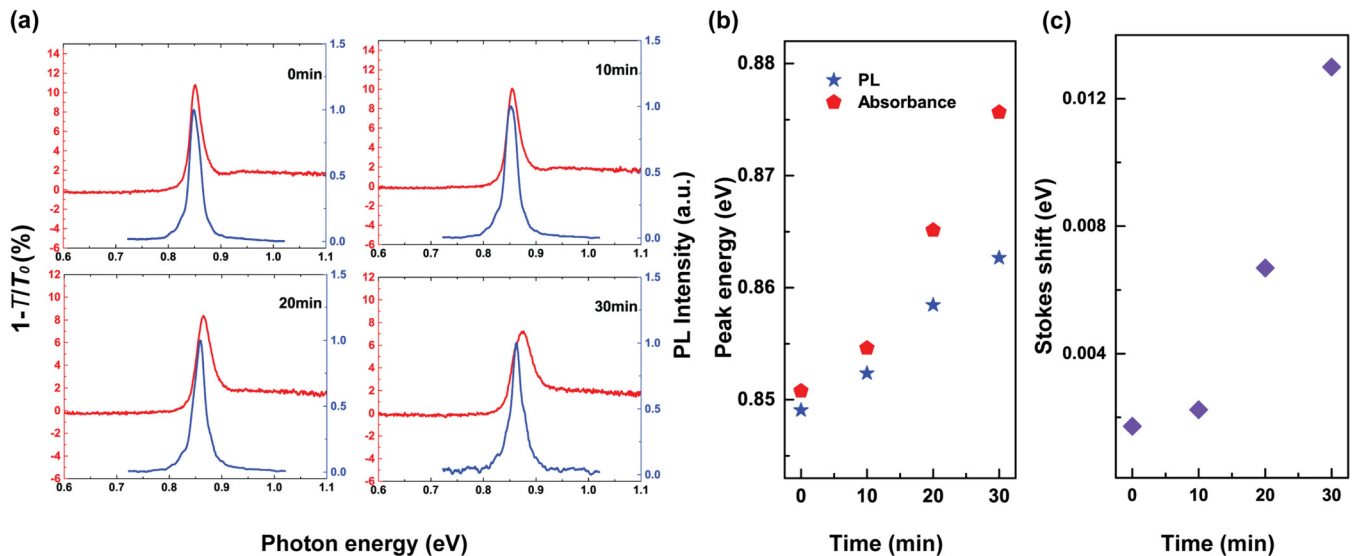

FIG. 4. Defect-induced Stokes shift. (a) Comparison of IR absorption and PL spectra of a 3L BP on the PDMS substrate. The spectra are shifted vertically for clarity. (b) Peak energies extract from (a). (c) Stokes shift during the degradation, indicating the accumulation of defects over time.
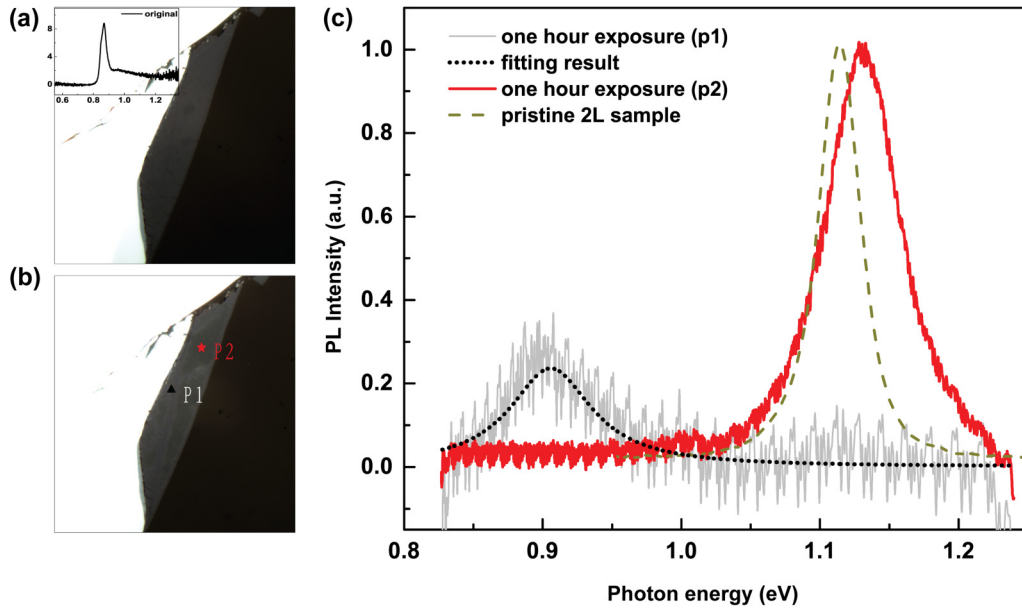
FIG. 5. Inhomogeneous layer thinning. (a) Optical microscope image of an original cleaved 3*L* BP sample on the PDMS substrate. Inset shows the IR absorption spectrum. (b) Optical microscope image of (a) after one hour exposure to air: P1 represents the location marked by a black triangle and P2 represents the location marked by a red star. (c) PL spectra of typical locations marked in (b). Two different peaks refer to 3*L* and 2*L* BP, respectively. A pristine 2*L* PL spectrum is shown for comparison.

samples (1*L* and 2*L*), our hypothesis is still valid to a large extent.

In spite of more defects, we can in principle take advantage of the controllable degradation for band-structure engineering. The band gap of pristine FL-BP cannot vary continuously when the layer number changes. However, in conjunction with controllable air exposure of the samples, additional continuous tuning of the band gap can be achieved and optical resonance is likely to cover a wide spectral range continuously with both pristine and slightly degraded FL-BP samples. The tuning of the band structure through oxidation can be applied to other 2D materials as well, as recently demonstrated in FL InSe [38]. As long as the effective mass of carriers in the *z* direction is relatively small, the tuning will be efficient. In this regard, FL-BP is a model system to demonstrate such tuning.

C. Stokes shift

In addition to blueshift of resonance peaks, the enhanced IR absorption and PL peak energy difference was also observed during our measurements. This energy difference, termed as the Stokes shift, is quite common in semiconductor optics [39]. Figure 4(a) shows a direct comparison of absorption and emission spectra for the same 3*L* sample, where each set of IR absorption and PL spectra was obtained under the same sample quality. The pristine sample showed narrow IR absorption and PL peaks, and their peak energies match well. Both the IR absorption peak and PL peak shift to higher energies after air exposure, as shown in Fig. 4(b). More importantly, a large redshift of PL peak energy relative to the IR absorption peak appeared after it was exposed to air, and the energy difference increased with increasing exposure time [see Fig. 4(c)]. It is associated with defects or impurity states below the band gap. The luminescence process favors the

lowest energy for recombination, and defect or impurity states below the band gap tend to attract the PL peak to the lower-energy side of the absorption peak. Therefore, the Stokes shift is an indicator of sample quality. The enhancement of the Stokes shift of our BP samples during air exposure is fully consistent with sample degradation.

D. Inhomogeneous thinning

After discussing the early stage of the degradation, we can now take a closer look at the later stage. Typically, the sample starts to visually show inhomogeneity under an optical microscope. Figure 5(a) shows a freshly cleaved 3*L*-BP sample; the layer number was verified by IR absorption spectrum [inset of Fig. 5(a)]. After one-hour exposure in air, areas with different optical contrast emerged [Fig. 5(b)], which indicates the thickness of the sample was reduced in certain areas. Indeed, PL spectra confirm this assertion. We collected PL spectra at locations marked by a black triangle (P1) and red star (P2), which refer to two different layer numbers according to the optical contrast. As shown in Fig. 5(c), the PL spectrum at P2 (red curve) has a peak at 1.15 eV which originates from a 2*L* BP. The slight blueshift from a pristine 2*L* BP (dashed line) might result from the early-stage oxidization. The PL peak at P1 (black curve), which is from the 3*L* part, is nearly quenched owing to a long-time exposure in air. These results demonstrate that the 3*L* sample partly turned into 2*L*, with the rest of 3*L* strongly degraded and the newly emerged 2*L* still of relatively high quality. The flake, therefore, constitutes two types of thickness simultaneously. Of course, this process keeps going and the thickness of the sample can be further reduced inhomogeneously. Eventually, the whole piece of the BP flake is decomposed, possibly leaving some faint vestiges. The spectrum of an original 5*L* sample with the coexistence

of 3, 4 and 5*L* BP after degradation is shown in the Supplement Material [34]. The coexistence of multiple peaks in the IR spectrum indicates the inhomogeneous degradation and sample-thickness reduction. Now a full picture of air exposure for FL-BP emerges: Initially, the top layer of a *N*-layer BP is slightly oxidized and a potential barrier forms between the top layer and the rest, which shifts the resonances to higher energy; with the reaction progressing, some parts of the oxidized top layer may be decomposed by moisture, leaving a relatively fresh *N*-1 layer coexisting with the degraded *N* layer; oxidation progresses further for the fresh *N*-1 layer and eventually the whole sample is decomposed.

IV. CONCLUSION

In summary, we demonstrated that air exposure has a strong effect on the electronic structure of BP. The band gap and higher-order subband transitions shift to higher energies. A quantum well model can well account for our observations. The signatures of early-stage degradation include blueshift and broadening of resonance peaks, as well as Stokes shift in PL. Later-stage degradation causes layer-number reduction, typically inhomogeneously. Our study not only provides a sensitive means to characterize the quality of BP samples, but also paves a way for band-structure tuning through controllable defect engineering.

[1] L. Li, Y. Yu, G. J. Ye, Q. Ge, X. Ou, H. Wu, D. Feng, X. H. Chen, and Y. Zhang, Nat. Nanotechnol. **9**, 372 (2014).

[2] F. Xia, H. Wang, and Y. Jia, Nat. Commun. **5**, 4458 (2014).

[3] X. Wang and S. Lan, Adv. Opt. Photon. **8**, 618 (2016).

[4] X. Wang, A. M. Jones, K. L. Seyler, V. Tran, Y. Jia, H. Zhao, H. Wang, L. Yang, X. Xu, and F. Xia, Nat. Nanotechnol. **10**, 517 (2015).

[5] P. Li and I. Appelbaum, Phys. Rev. B **90**, 115439 (2014).

[6] L. Li, J. Kim, C. Jin, G. J. Ye, D. Y. Qiu, F. H. da Jornada, Z. Shi, L. Chen, Z. Zhang, F. Yang, K. Watanabe, T. Taniguchi, W. Ren, S. G. Louie, X. H. Chen, Y. Zhang, and F. Wang, Nat. Nanotechnol. **12**, 21 (2016).

[7] T. Low, A. S. Rodin, A. Carvalho, Y. Jiang, H. Wang, F. Xia, and A. H. Castro Neto, Phys. Rev. B **90**, 075434 (2014).

[8] A. N. Rudenko and M. I. Katsnelson, Phys. Rev. B **89**, 201408 (2014).

[9] H. Liu, A. T. Neal, Z. Zhu, Z. Luo, X. Xu, D. Tománek, and P. D. Ye, ACS Nano **8**, 4033 (2014).

[10] J. Qiao, X. Kong, Z. X. Hu, F. Yang, and W. Ji, Nat. Commun. **5**, 4475 (2014).

[11] Y. Huang, J. Qiao, K. He, S. Bliznakov, E. Sutter, X. Chen, D. Luo, F. Meng, D. Su, J. Decker, W. Ji, R. S. Ruoff, and P. Sutter, Chem. Mater. **28**, 8330 (2016).

[12] W. Luo, D. Y. Zemlyanov, C. A. Milligan, Y. Du, L. Yang, Y. Wu, and P. D. Ye, Nanotechnology **27**, 434002 (2016).

[13] S. Walia, Y. Sabri, T. Ahmed, M. R. Field, R. Ramanathan, A. Arash, S. K. Bhargava, S. Sriram, M. Bhaskaran, V. Bansal, and S. Balendhran, 2D Mater. **4**, 015025 (2016).

[14] G. Wang, W. J. Slough, R. Pandey, and S. P. Karna, 2D Mater. **3**, 025011 (2016).

[15] T. Zhang, Y. Wan, H. Xie, Y. Mu, P. Du, D. Wang, X. Wu, H. Ji, and L. Wan, J. Am. Chem. Soc. **140**, 7561 (2018).

[16] T. Ahmed, S. Balendhran, M. N. Karim, E. L. H. Mayes, M. R. Field, R. Ramanathan, M. Singh, V. Bansal, S. Sriram, M. Bhaskaran, and S. Walia, npj 2D Mater. Appl. **1**, 18 (2017).

[17] C. Zhao, M. C. Sekhar, W. Lu, C. Zhang, J. Lai, S. Jia, and D. Sun, Nanotechnology **29**, 245202 (2018).

[18] W. Luo and H. Xiang, Angew. Chem. Int. Ed. **55**, 8575 (2016).

[19] S. Walia, S. Balendhran, T. Ahmed, M. Singh, C. El-Badawi, M. D. Brennan, P. Weerathunge, M. N. Karim, F. Rahman, A. Rassell, J. Duckworth, R. Ramanathan, G. E. Collis, C. J. Lobo, M. Toth, J. C. Kotsakidis, B. Weber, M. Fuhrer, J. M. Dominguez-Vera, M. J. S. Spencer, I. Aharonovich, S. Sriram, M. Bhaskaran, and V. Bansal, Adv Mater. **29**, 1700152 (2017).

[20] J. Pei, X. Gai, J. Yang, X. Wang, Z. Yu, D. Y. Choi, B. Luther-Davies, and Y. Lu, Nat. Commun. **7**, 10450 (2016).

[21] S. Lin, Y. Li, W. Lu, Y. S. Chui, L. Rogée, Q. Bao, and S. P. Lau, 2D Mater. **4**, 025001 (2017).

[22] S. Kuriakose, T. Ahmed, S. Balendhran, V. Bansal, S. Sriram, M. Bhaskaran, and S. Walia, 2D Mater. **5**, 032001 (2018).

[23] J. O. Island, G. A. Steele, H. S. J. v. d. Zant, and A. Castellanos-Gomez, 2D Mater. **2**, 011002 (2015).

[24] D. Grasseschi, D. A. Bahamon, F. C. B. Maia, A. H. C. Neto, R. O. Freitas, and C. J. S. de Matos, 2D Mater. **4**, 035028 (2017).

[25] J. Plutnar, Z. Sofer, and M. Pumera, ACS Nano **12**, 8390 (2018).

[26] A. Favron, E. Gaufres, F. Fossard, A. L. Phaneuf-L'Heureux, N. Y. Tang, P. L. Levesque, A. Loiseau, R. Leonelli, S. Francoeur, and R. Martel, Nat Mater. **14**, 826 (2015).

[27] F. Alsaffar, S. Alodan, A. Alrasheed, A. Alhussain, N. Alrubaiq, A. Abbas, and M. R. Amer, Sci. Rep. **7**, 44540 (2017).

[28] H. B. Ribeiro, M. A. Pimenta, C. J. S. de Matos, R. L. Moreira, A. S. Rodin, J. D. Zapata, E. z. A. T. de Souza, and A. H. C. Neto, ACS Nano **9**, 4270 (2015).

[29] H. B. Ribeiro, M. A. Pimenta, and C. J. S. de Matos, J. Raman Spectrosc. **49**, 76 (2017).

[30] A. L. Phaneuf-L'Heureux, A. Favron, J. F. Germain, P. Lavoie, P. Desjardins, R. Leonelli, R. Martel, and S. Francoeur, Nano Lett. **16**, 7761 (2016).

[31] X. Luo, X. Lu, G. K. Koon, A. H. Castro Neto, B. Ozyilmaz, Q. Xiong, and S. Y. Quek, Nano Lett. **15**, 3931 (2015).

[32] G. Zhang, S. Huang, A. Chaves, C. Song, V. O. Ozcelik, T. Low, and H. Yan, Nat. Commun. **8**, 14071 (2017).

[33] G. Zhang, A. Chaves, S. Huang, F. Wang, Q. Xing, T. Low, and H. Yan, Sci. Adv. **4**, eaap9977 (2018).

[34] See Supplemental Material at http://link.aps.org/supplemental/10.1103/PhysRevB.99.075427 for efficient nitrogen protection, additional typical air-exposed samples, additional data for inhomogeneous layer thinning, and quantum well model.

[35] A. Ziletti, A. Carvalho, D. K. Campbell, D. F. Coker, and A. H. Castro Neto, Phys. Rev. Lett. **114**, 046801 (2015).

[36] A. Castellanos-Gomez, L. Vicarelli, E. Prada, J. O. Island, K. L. Narasimha-Acharya, S. I. Blanter, D. J. Groenendijk, M. Buscema, G. A. Steele, J. V. Alvarez, H. W. Zandbergen, J. J. Palacios, and H. S. J. van der Zant, 2D Mater. **1**, 025001 (2014).

[37] Q. Zhou, Q. Chen, Y. Tong, and J. Wang, Angew. Chem. Int. Ed. **55**, 11437 (2016).

[38] N. Balakrishnan, Z. R. Kudrynskyi, E. F. Smith, M. W. Fay, O. Makarovsky, Z. D. Kovalyuk, L. Eaves, P. H. Beton, and A. Patanè, 2D Mater. **4**, 025043 (2017).

[39] C. Ruppert, O. B. Aslan, and T. F. Heinz, Nano Lett. **14**, 6231 (2014).